International Journal of Concrete Structures and Materials

RESEARCH

Open Access

Bending Behavior of RC Beams with Regular Web Openings and Non-corroding GFRP Reinforcement

Saruhan Kartal[1*] and Emin Kısıklı[2]

Abstract

The present study pertains to the flexural behavior of RC beams with openings and non-metallic (GFRP) reinforcement. The main goal of preferring GFRP reinforcement over the conventional steel reinforcement was to safeguard the beams against the reinforcement corrosion. The presence of multiple regular transverse openings throughout the beam length increases the susceptibility of reinforcing bars to corrosion as the larger contact area in these beams with the outside environment increases the ingress of corrosive agents. Within the scope of the study, a total of 8 RC beams, including two reference beams without web openings, were tested under four-point bending. The test parameters were the flexural reinforcement ratio, the presence of short stirrups in the chords, and the presence of diagonal reinforcement spiraling around the openings. Since GFRP stirrups are difficult to bend, each stirrups was formed by connecting four individual FRP bars around the longitudinal bars. The opening circular geometry was adopted to avoid stress concentrations around the sharp corners of opening and to facilitate the placement and fixing of different schemes of reinforcement in the beams. The present tests depicted that the diagonal reinforcement around the openings have considerable contribution to the flexural behavior of RC beams with GFRP reinforcement and with multiple regular transverse openings. The RC beams with openings were able to approach their analytical flexural capacities in the presence of diagonal reinforcement for both moderately and heavily reinforced beam groups. The analytical deflection predictions of GFRP-RC beams with openings showed a good agreement with experimental data.

Keywords GFRP RC beams with web openings, Shear failure, Circular opening, Post, Chord

1 Introduction

Modern structures are equipped with various kinds of services for the inhabitants, including but not limited to power, water, sewage, and ventilation systems. The presence of all these systems can cause the use of an important volume of the structure for various ducts, pipes, cables and fixtures associated with these services. In an attempt to increase the amount of usable space of the structure, transverse openings in the beam allowing the passage of these service components within the floor height are adopted in the original beam design or in the construction stage (Fig. 1a). The random drilling of web openings, not present in the original design, might lead to a reduction in both rigidity and strength of RC beams. This application may result in non-ductile failure modes, such as shear failure or Vierendeel panel action, causing the RC beams to collapse before reaching their bending capacities (Wojdak, 2013). The proximity of openings to beam–column joints increases the likelihood of the undesirable failure modes (Amin et al., 2021). To reduce

Journal information: ISSN 1976- 0485 / eISSN 2234-1315.

*Correspondence:
Saruhan Kartal
saruhankartal@kku.edu.tr
[1] Department of Civil Engineering, Kirikkale University, 71451 Kirikkale, Turkey
[2] Institute of Science, Kirikkale University, 71451 Kirikkale, Turkey

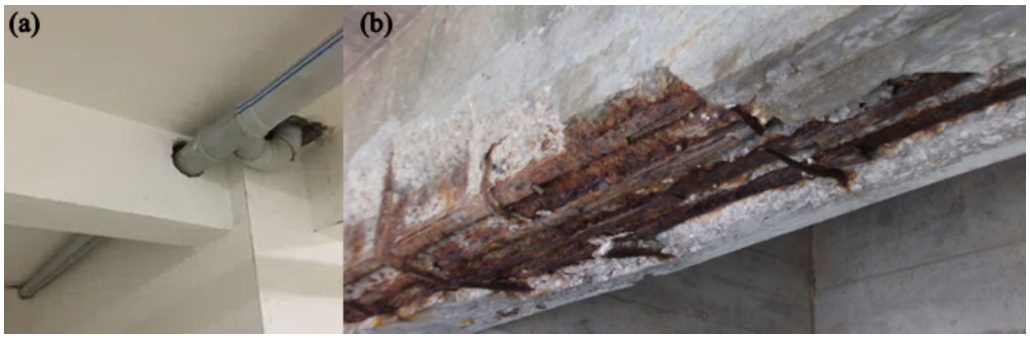

Fig. 1 **a** Randomly drilling of holes in hardened beams and passing these systems through the holes, **b** corrosion of steel reinforcement

the aforementioned negative effects, it is recommended to integrate RC beams with openings during the design phase of a structure rather than post-drilling.

Numerous researchers have conducted studies within this scope, focusing on RC beams with either a single or multiple openings in the shear spans. According to Mansur et al. (1991), RC beams with a large opening in the shear span exhibit a Vierendeel-type failure, with an increasing tendency of this type of failure mode as the size of the openings increases. Mansur et al. (1992) proposed a reduction in both bending and shear rigidities when predicting deflections in RC beams with a single large opening. In addition, Tan and Mansur (1996) introduced design guidelines specifying the size and location of these openings. Mansur (1998, 1999) established distinct shear failure modes for both beam and frame types in RC beams with web openings. Furthermore, a differentiation was made between small and large openings based on the structural behavior observed. Tan et al. (2001) illustrated the benefits of diagonal reinforcement around openings in T-beams. El-Kareim et al. (2020) conducted an investigation on RC deep T-beams with rectangular openings. The dimensions of the openings were selected as parameters, demonstrating their significant influence on the strength and rigidity of the flange.

Many research findings indicate that the behavior of reinforced concrete (RC) beams with a limited number of web openings is primarily influenced by various shear failure modes. This is attributed to stress concentrations around the openings. In order to prevent the mentioned failures, it has been recommended in some studies to create numerous regular openings along the beam and distribute the stress around these openings. Aykaç and Yılmaz (2011) and Aykaç et al., (2013, 2014) investigated the shear and flexural behavior of RC beams with different opening geometries and special reinforcement details. The results obtained from tests on RC beams with circular openings and diagonal reinforcement have shown that it is possible to achieve flexural capacity. Meanwhile, Kalkan (2014) proposed analytical equations for predicting the deformations of these beams. In addition, Kalkan et al. (2021) suggested coefficients for deformation calculations based on different opening geometries.

Another shortcoming of the presence of the web openings in the beams is the increase in the susceptibility of RC beams to reinforcement corrosion due to the increase in the exposed surfaces of the beams to outside environment. An effective solution for the reinforcement corrosion is the adoption of non-metallic reinforcing bars, particularly the FRP ones, in the beams with openings. FRP fabrics have gained popularity in recent years due to their resistance to corrosion, high tensile strengths, and ease of application. Within this scope, recent studies on RC beams with openings aim to increase their shear strengths through FRP wrapping. Abdel-Kareem (2014) applied FRP wraps in various configurations. Furthermore, a modification has been suggested for the available analytical equations. Lu et al. (2015) conducted a study on the bending behavior of RC beams with openings, strengthened through the external bonding of CFRP layers. The application of CFRP layers in the vertical direction demonstrated a higher contribution to shear strength compared to application in the horizontal direction. Nie et al. (2018) has developed a new seismic strengthening method for T-section RC beams with the aim of achieving a strong column–weak beam hierarchy. By creating an opening in the beam body, the bending capacity is reduced, and the shear capacity is increased through CFRP wrapping. For ductile behavior, it is necessary to completely wrap the lower chord. In addition, on the the remaining beam body without opening was applied CFRP U-wrapping. Salih et al. (2020) conducted tests on RC beams with circular opening under cyclic loading. Different configurations of CFRP wrapping were applied around the opening on the beam body. Strength and ultimate deformation capacities increased by approximately 67% and 77%, respectively. Elansary et al. (2022)

examined the bending behavior of RC beams with rectangular openings near the supports. In specimens without CFRP wrapping, there was an approximately 43% loss compared to the solid element, while shear capacity significantly increased by approximately 95% with CFRP wrapping. Almusallam et al. (2018) investigated the effect of CFRP wrapping on RC beams with large rectangular opening in the bending region. Strengthening details, opening dimensions, and loading types were defined as parameters. In specimens where the upper chord depth was greater than the equivalent depth of the rectangular compression block, there was no change in bending capacity. Nie et al. (2020) investigated the effectiveness of different types of CFRP wrapping in beams with rectangular web openings. In numerical studies, elements where the upper and lower chords and the posts around the opening were completely wrapped yielded the best results. Elsanadedy et al. (2019) conducted an experimental and numerical study on RC beams with large rectangular openings in the shear regions. GFRP wrapping was also applied along with CFRP, and the effectiveness of anchoring FRP fabrics with steel plates was investigated.

The corrosion of steel reinforcement (Fig. 1b) leads to cross-sectional losses and a decrease in structural performance (Cairns et al., 2005; Imperatore et al., 2009, 2017). Carlo et al. (2023) investigated the flexural behavior of beams exposed to corrosion at different rates. Due to corrosion, ductility, ultimate deformation, and strength values showed significant decreases. With an increase in the corrosion rate, bond failures and cases of steel reinforcement rupture were encountered. Adhesion losses due to corrosion also adversely affect structural behavior (Coccia et al., 2016; Coronelli, 2002). Fiber-reinforced polymer reinforcements (FRP reinforcement) are considered the most significant alternative to steel reinforcements due to their high corrosion resistance, and their usage is increasing day by day. In addition, FRP reinforcements have many advantages, such as high tensile strength, lightweight, and non-magnetic properties.

A detailed examination of the literature reveals that using regular openings in the beam web and special reinforcement details allow specimens to achieve bending capacity, exhibit sufficient ductility, and demonstrate the performance at the serviceability limit state. Furthermore, reinforcing the openings by wrapping them has also yielded similar results. The corrosion occurs in structures due to leaks, water infiltrations, and other reasons in water installations. In the literature, the studies related to RC beams with openings, steel reinforcements were used, and an effective solution against corrosion could not be identified.

It is known that corrosion effects are particularly pronounced in basement and ground floors, where power, water, sewage, and ventilation systems converge. In addition, in this region, due to seismic effects, overturning moments and shear forces are also significant. RC beams with weakened structural performance due to openings will experience even more pronounced losses when exposed to corrosion. Accordingly, in the present study, RC beams with regular circular openings were produced using only FRP reinforcements differing from the other studies in the literature. The main aim was to obtain RC beams with regular openings that are effective against corrosion and can accommodate utilities (pipes and channels). In this context, the effects of different parameters (longitudinal reinforcement ratio, stirrups in the posts, and diagonal reinforcements between openings) on the flexural behavior, strength, and failure mode of GFRP-RC beams with regular circular openings were investigated.

2 Experimental Study

2.1 Test Specimens and Material Properties

Mansur (2006) made a definition of small and large openings based on structural behavior. The opening was categorized as large if the ratio of the opening height to the beam height is greater than 0.40, and as small if it is less than 0.40. In the present study, this ratio was selected as 0.48 (large opening). In addition, a circular opening geometry without sharp corners has been preferred, as it minimizes losses in both rigidity and strength (Tan et al., 2001; Aykaç & Yılmaz, 2011; Aykaç et al., 2013, 2014).

In the experimental study, a total of eight RC beams were prepared. Each beam had a width of 200 mm, a height of 336 mm, and a total length of 3000 mm, with a clear span of 2800 mm. The study consists of two groups based on whether the reinforcement ratio is moderately or heavily. The main parameters were determined as the reinforcement ratio, the use of short stirrups in the posts, and the use of diagonal reinforcement between openings. Each experimental group included reference beams without openings, and the remaining RC beams had a total of 10 circular openings (Ø160 mm) along the span. The fabrication GFRP stirrups in the desired dimensions could not be obtained. Therefore, the stirrups were prepared by connecting four individual GFRP bars (Ø8) with tie wire.

Special reinforcement details were utilized in all test specimens to prevent different types of shear failures. All test specimens had short GFRP stirrups (Ø8/6 mm) at the upper and lower chords. In the constant moment region (Fig. 2a-a, cross section), there were a total of five and six GFRP (Ø12) rebars as tension reinforcement, for the moderately and heavily reinforcement, respectively. In other words, the moderate ($\rho_f/\rho_{fb}=2.57$) and heavily ($\rho_f/\rho_{fb}=3.05$) reinforcement ratios were approximately 2.57 and 3.05 times the balanced reinforcement ratio (ρ_{fb})

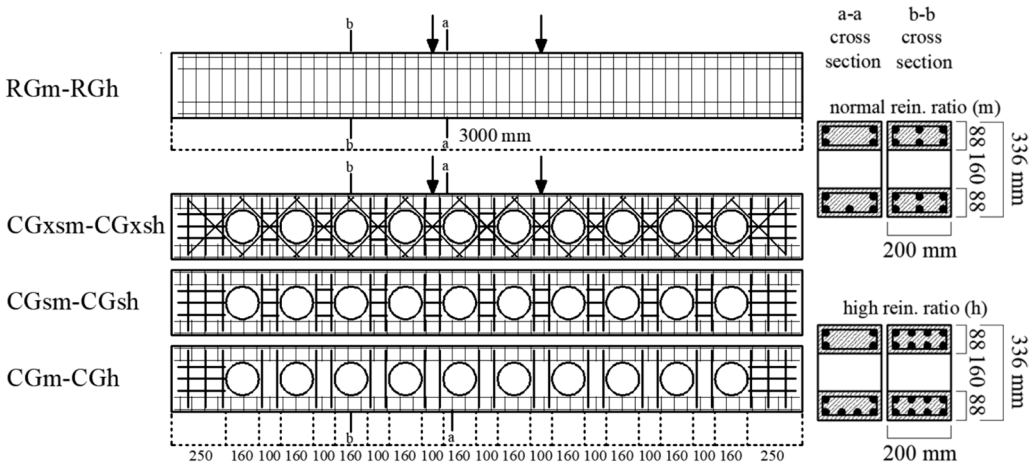

Fig. 2 Reinforcement details of the specimens

according to ACI 440.1R-15 (2015). In this way ($\rho f > \rho fb$), the RC beams were ensured to be designed as over-reinforced, meaning that the crushing of concrete preceded the rupture of FRP reinforcement. In the same region of the upper chord, two pairs of internal and external compression reinforcement were used.

Vierendeel panel action behavior is a brittle failure mode commonly observed in RC beams with one/multiple openings. Before RC beams reach their bending capacity, shear forces cause the formation of a total of four plastic hinges (resulting in additional rotations) in the upper and lower chords of the openings, leading to the development of a collapse mechanism. The additional longitudinal reinforcements were utilized to prevent Vierendeel panel action type failure in the shear regions (Fig. 2b-b, cross section). The use of these additional reinforcements was aimed to enhance the bending capacity of the chords, thereby preventing the formation of plastic hinges. The specimens with heavily and moderately reinforcement ratios, there were a total of five and three Ø12 mm GFRP longitudinal reinforcement in the inner and outer layers of both the lower and upper chord members, respectively.

The diagonal reinforcement and longitudinal reinforcements in the posts and chords were preferred as 12 mm diameter GFRP bars. The details about the test specimens is presented in Table 1, while the reinforcement details is shown in Fig. 2. In the nomenclature, the initial capital letter "R" is used for reference specimens without openings, while "C" is used for RC beams with circular openings. The second capital letter "G" indicates that the specimens are reinforced with only GFRP materials. In lowercase letters, "x" and "s" signify the use of diagonal reinforcement between the openings and short stirrups in the posts, respectively, while "m" and "h" indicate the moderately and high reinforcement ratios, respectively.

All test specimens were prepared by single pouring the concrete. Due to the use of excessive reinforcement in the chords and posts, a superplasticizer admixture and aggregate with a maximum size of 11.2 mm were preferred to allow the concrete to easily settle into the molds. The average compressive strength

Table 1 Test specimens

Group No	Beam	Opening Type	Reinforcement ratio	Diagonal reinforcement	Stirrups in the posts
1	RGm	–	Moderately	–	–
	CGm	Circular	Moderately	–	–
	CGsm	Circular	Moderately	–	✓
	CGxsm	Circular	Moderately	✓	✓
2	RGh	–	Heavily	–	–
	CGh	Circular	Heavily	–	–
	CGsh	Circular	Heavily	–	✓
	CGxsh	Circular	Heavily	✓	✓

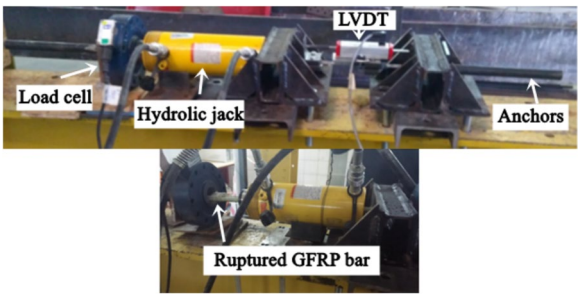

Fig. 3 Tensile test setup for GFRP reinforcement

Table 2 Mechanical properties of GFRP reinforcement

Diameter (mm)	Modulus of Elasticity (GPa)	Tensile Stength (MPa)
8	42	787
12	55	924

of 20 cylindrical samples (150 × 300 mm) taken from fresh concrete was 31.32 MPa. The tensile test setup for GFRP reinforcement is illustrated in Fig. 3, and the mechanical properties are provided in Table 2.

The stages of the specimen preparation and the details of reinforcement are illustrated in Fig. 4. In the first step, molds were prepared. Subsequently, circular pipes were mounted in the molds for the openings. Secondly, reinforcement were prepared for each element and placed in the molds. Finally, concrete was poured, and the test specimens were cured with tap water for seven days.

2.2 Test Setup

All tests were carried out at the Structural Mechanics Laboratory of Kırıkkale University. The load was applied to the system through a hydraulic jack connected to a frame with a capacity of 250 kN, and it was measured using a load cell. The simply supported beams were loaded at two points through a load-spreader beam. The support points were located 100 mm from the ends of the beam, while the load points were located 250 mm from the midpoint of the beam. In addition, *a/d* (shear span to effective depth) ratio were determined to be approximately 3.8. The vertical deformations were measured by means of six transducers with a capacity of 150/250 mm. Four of them were connected to the beam at the load and support points. The remaining two were connected to the front and rear faces of the beam at midspan to detect any twisting rotations arising from the undesired eccentric loading. The vertical deflections at midspan were obtained from the average of these two measurement values. The load and deflection measurements were recorded by a data acquisition system and stored on a computer. The test setup are illustrated in Fig. 5.

3 Experimental Results and Discussion

3.1 Failure Modes

The failure mode of the test specimens are provided in Figs. 6, and 7. The reference RGm was the only test specimen that reaches the bending moment capacity. In the constant moment region, concrete had crushed, exhibiting behavior of an over RC beam ($\rho_f > \rho_{fb}$). After the initiation of conrete crushing, shear and debonding cracks developed. Similar to the findings of Kytinou et al. (2022), the slippage of longitudinal reinforcements did not affect the type of failure or the bending behavior.

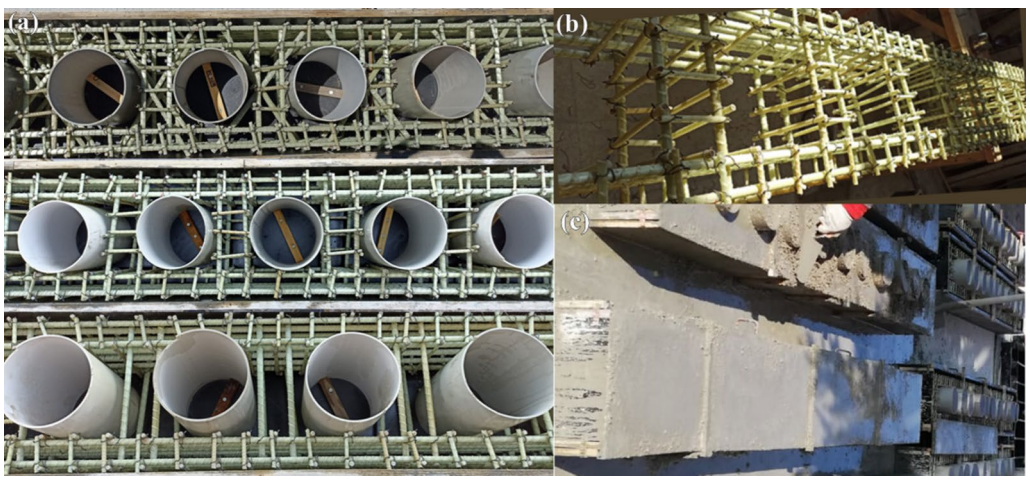

Fig. 4 Preparation stages of the test specimens: **a** reinforcement details, **b** reinforcement skeleton, **c** batching concrete

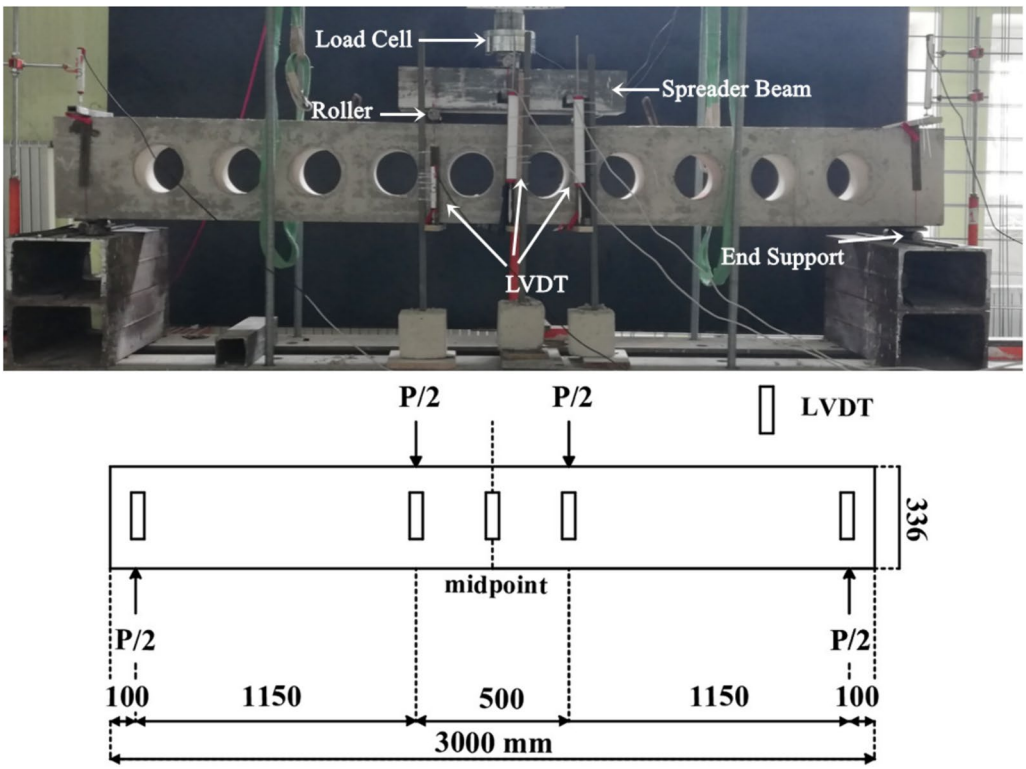

Fig. 5 Test setup

In the test specimen RGh, the main shear crack developed before crushing of concrete and progressed towards the compression zone, leading to simultaneous diagonal shear and debonding failure. This type of failure triggerred concrete crushing and the compression rebars buckled. Although stirrups (Ø8/60 mm) were frequently used to reach the bending capacity, their being prepared by connecting four individual GFRP bars did not prevent shear failure. None of the RC beams with openings reached the bending capacity. In all of them, diagonal compression struts formed between the lower and upper chords. resulting in crushing in the shear zone. Beam type and debonding failure between the tensile reinforcement concrete were observed. The reasons for this type of failure include the individual of short stirrups, the low dowel action effect of GFRP longitudinal reinforcement, and the significant role of openings in the web. As the load level increases, in the layer of longitudinal reinforcement near the openings in the lower and upper chords, observed losses in bond occurred due to the presence of openings, and debonding cracks developed parallel to the longitudinal axis of the beam. Particularly in CGm, CGsm, CGh, and CGsh specimens, debonding failure became prominent at failure stage. The bond failure resulted in the pullout of small individual stirrups located in the chords. However, there was no damage observed in the posts. Furthermore, similar to Kartal (2024), Vierendeel type shear failure did not observe in any of the RC beams with regular circular openings.

CGxsm and CGxsh test specimens, which include diagonal reinforcement between openings, were the test specimens that have yielded closest results to the bending capacities, and limited damage was observed compared to other RC beams. Diagonal reinforcements in both directions served as tension and compression struts, delaying shear-type failure in the beam. In addition, diagonal reinforcements prevented the progression of debonding cracks, ensuring limited damage (Tan et al., 2001; Aykaç & Yılmaz, 2011; Aykaç et al., 2013, 2014).

The increase in longitudinal reinforcement ratio did not cause a difference in failure modes in RC beams with openings, while in reference specimens, it caused the failure mode to change from bending to bond + shear failure. This situation is thought to be due to local weaknesses in the concrete and/or FRP reinforcement.

In the present study, first cracking was observed at low load levels in all beams, and the crack depth reached significant values. The low modulus of elasticity of FRP reinforcement compared to steel reinforcement causes serviceability limit state problems (deformation and cracking). In order to overcome this problem in RC beams, Wei et al. (2024) and Kartal

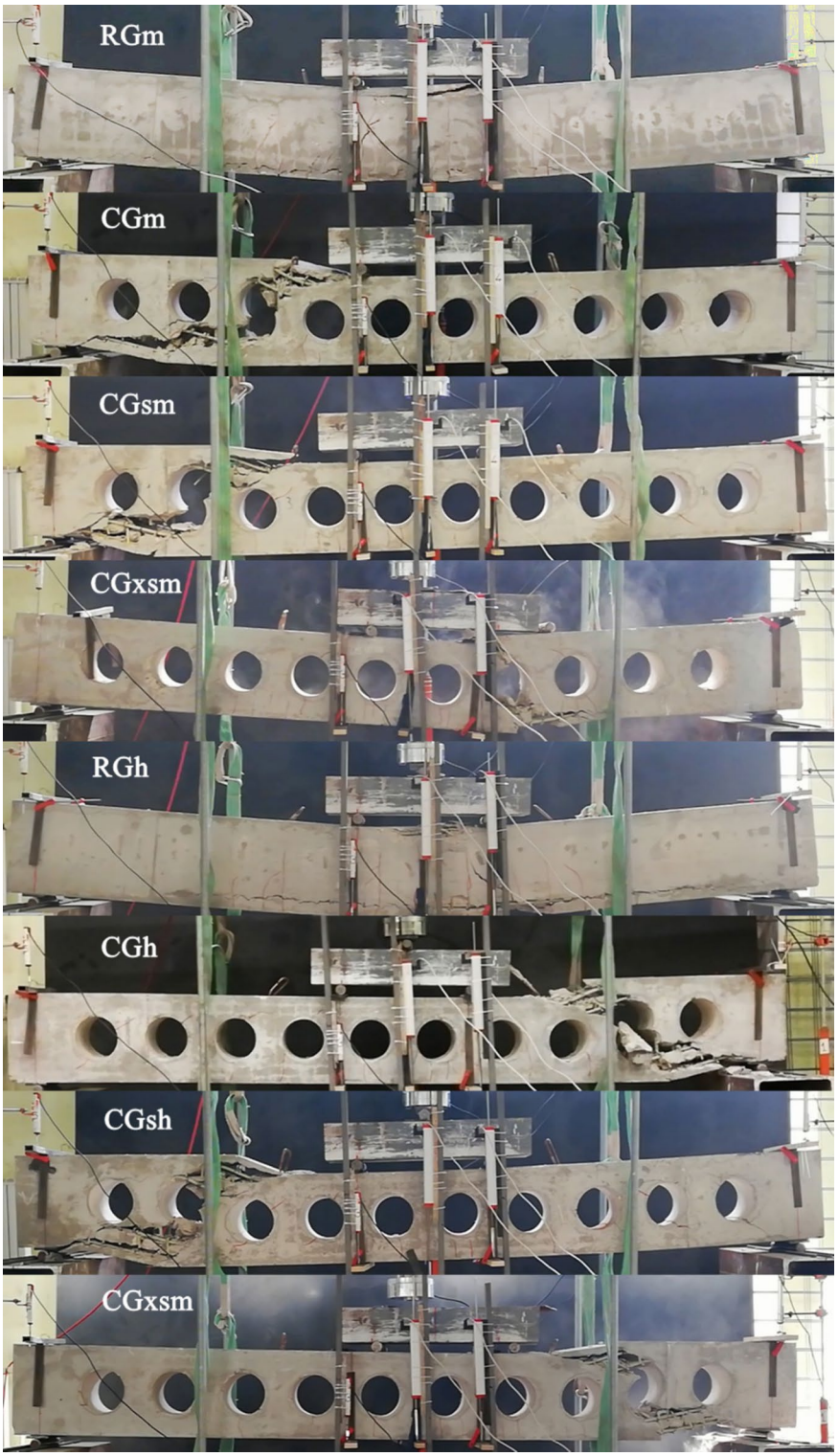

Fig. 6 Failure modes of the RC beams

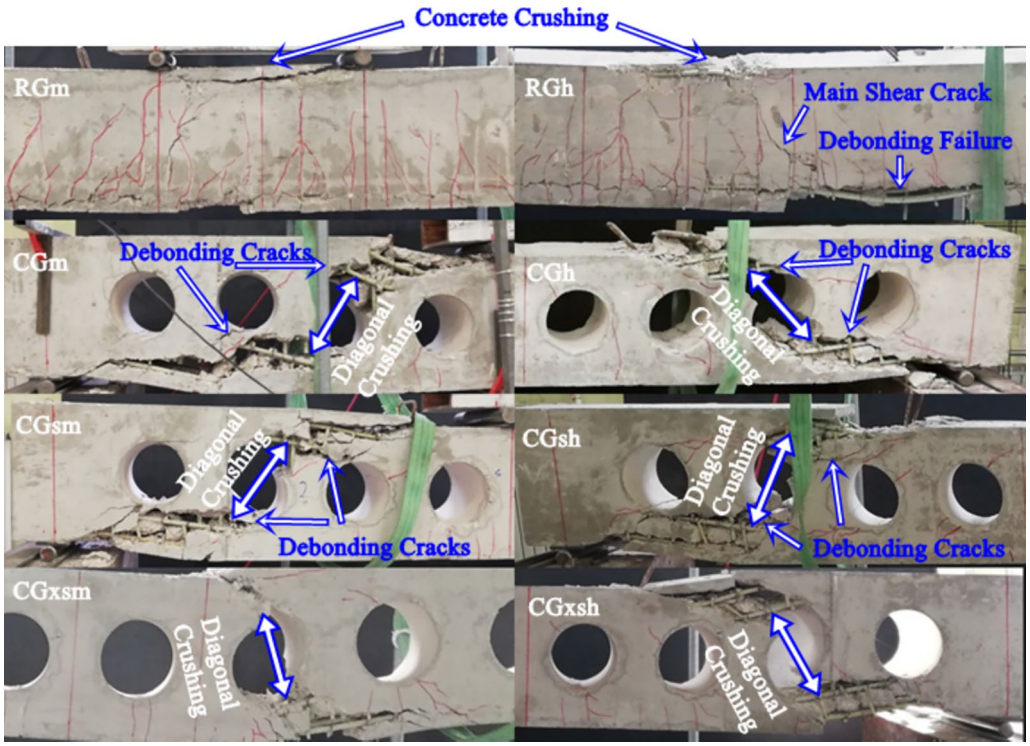

Fig. 7 Failure modes of the RC beams

et al. (2023) stated that FRP reinforcements should be used together with steel reinforcements, while Yang et al. (2024) and Koura et al. (2024) suggested that different types of fibers should be used. In addition, Kartal et al. (2021) stated that the predicted first cracking load of FRP-RC beams is significantly lower than the experimental data, which poses a major drawback for structural safety. In addition, it has been suggested that increasing the reinforcement ratio could be a solution to this problem.

3.2 Ultimate Loads, Rigidities and Energy Dissippation Capacities

The load–deflection curves of the test specimens are given in Fig. 8. All of them were approximately linear after the first cracking. In RC beams with openings, the load abruptly dropped due to brittle shear failure. However, in RGm and RGh, the load–deflection curve became horizontal with the beginning of concrete crushing and upon the completion of crushing, the load dropped suddenly.

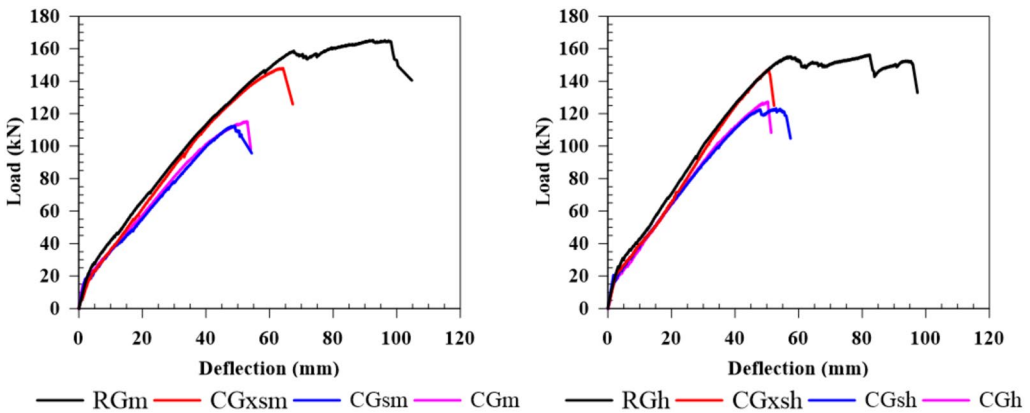

Fig. 8 Load–deflection curves of the test specimens

The rigidities (R), energy dissippation capacities (E_t) and ultimate load capacities (P_{max}) are presented in Table 3. The beam rigidity is defined as the slope of the line passing through the points corresponding to the onset of the load–deformation curve and 70% of the load capacity. The energy dissippation capacity corresponds to the total area under the load–deformation curve. In the calculations, the point where a 15% decrease observed after reaching the load capacity has been taken into account as the limiting value. In both experimental groups, the rigidity, energy dissippation and load capacities of the specimens without openings (RGm and RGh) were the highest.

The rigidity of the test specimens with diagonal reinforcement (CGxsm and CGxsh) was approximately the same as that of the specimens witout openings [R_r/R_s *(%)* value 101.07 and 97.57, respectively]. The load capacities of CGxsm and CGxsh were about to 10% and 5% lower, as compared to the realated reference specimens, respectively. The specimens without diagonal reinforcement had the lowest rigidity and load capacities within their respective experimental groups.

The presence or absence of short stirrups in the posts was not shown a significant effect on the relevant parameters. The main reason for this can be attributed to the low confinement effect of individual stirrups. In each experimental group, the energy dissippation capacities of the specimens with openings were significantly lower compared to the reference specimens as a result of the shear failure.

In the first experimental group, the losses between approximately 50% and 71%, while in the second experimental group, the losses between approximately 59% and 65%. The reason for the lower variability in the second experimental group is the occurrence of shear failure in the RGh test specimen simultaneously with concrete crushing.

In Fig. 9, load–deflection curves are given to examine the effects of the longitudinal reinforcement ratio parameter on test specimens with the same reinforcement details. The rigidity, load, and energy dissippation capacities of these elements have been compared in Table 4. An increase in the longitudinal reinforcement ratio resulted in a slight increase in rigidity for all test specimens.

In the reference specimens, an increase in the reinforcement ratio resulted in an approximate 6% decrease in load capacity, an approximately 7% decrease in energy dissippation capacity, while rigidity exhibited an approximate 17% increase. In RC beams without stirrups and diagonal reinforcement (CGm and CGh), about to 16% increase in rigidity, about to 11% increase in load capacity and about to 1.5% increase in their energy dissippation capacities were observed with increasing the reinforcement raito. When comparing the CGsm and CGsh specimens, an increase in the reinforcement ratio resulted in an approximate 10% increase in load capacity, approximately 23% increase in energy dissippation capacity, and approximately 12% increase in rigidity. On the other hand, comparing the test specimens with stirrups and diagonal

Table 4 Effects of longitudinal reinforcement ratio on related parameters

Parameter	Sh/Sm	Ratio of related parameters		
		R (%)	E_t (%)	P_{max} (%)
without openings	RGh/RGm	117.08	92.30	93.92
without stirrups in the posts	CGh/CGm	116.34	101.42	110.53
with stirrups in the posts	CGsh/CGsm	111.44	122.57	109.50
with stirrups in the posts and diagonal reinforcement	CGxsh/CGxsm	113.03	71.63	99.30

Sh—beam with high reinforcement ratio

Sm—beam with normal reinforcement ratio

Table 3 Rigidities, ultimate load and energy dissippation capacities of the test specimens

Group	Beam	*R (kN/mm)*	E_t *(kJ)*	P_{max} *(kN)*	R_r/R_s *(%)*	E_r/E_s *(%)*	P_r/P_s *(%)*
1st	RGm*	2.81	12.30	165.33	100.00	100.00	100.00
	CGm	2.57	3.84	115.24	91.46	31.25	69.70
	CGsm	2.71	3.76	112.52	96.44	30.54	68.06
	CGxsm	2.84	6.08	147.98	101.07	49.46	89.50
2nd	RGh*	3.29	11.35	155.27	100.00	100.00	100.00
	CGh	2.99	3.90	127.37	90.88	34.34	82.03
	CGsh	3.02	4.61	123.21	91.79	40.56	79.35
	CGxsh	3.21	4.36	146.95	97.57	38.39	94.64

* Reference specimen in each test group

R_r, E_r and P_r is the rigidity, energy dissippation and load capacity of reference specimen in each test group

R_s, E_s and P_s is the rigidity, energy dissippation and load capacity of the specimen

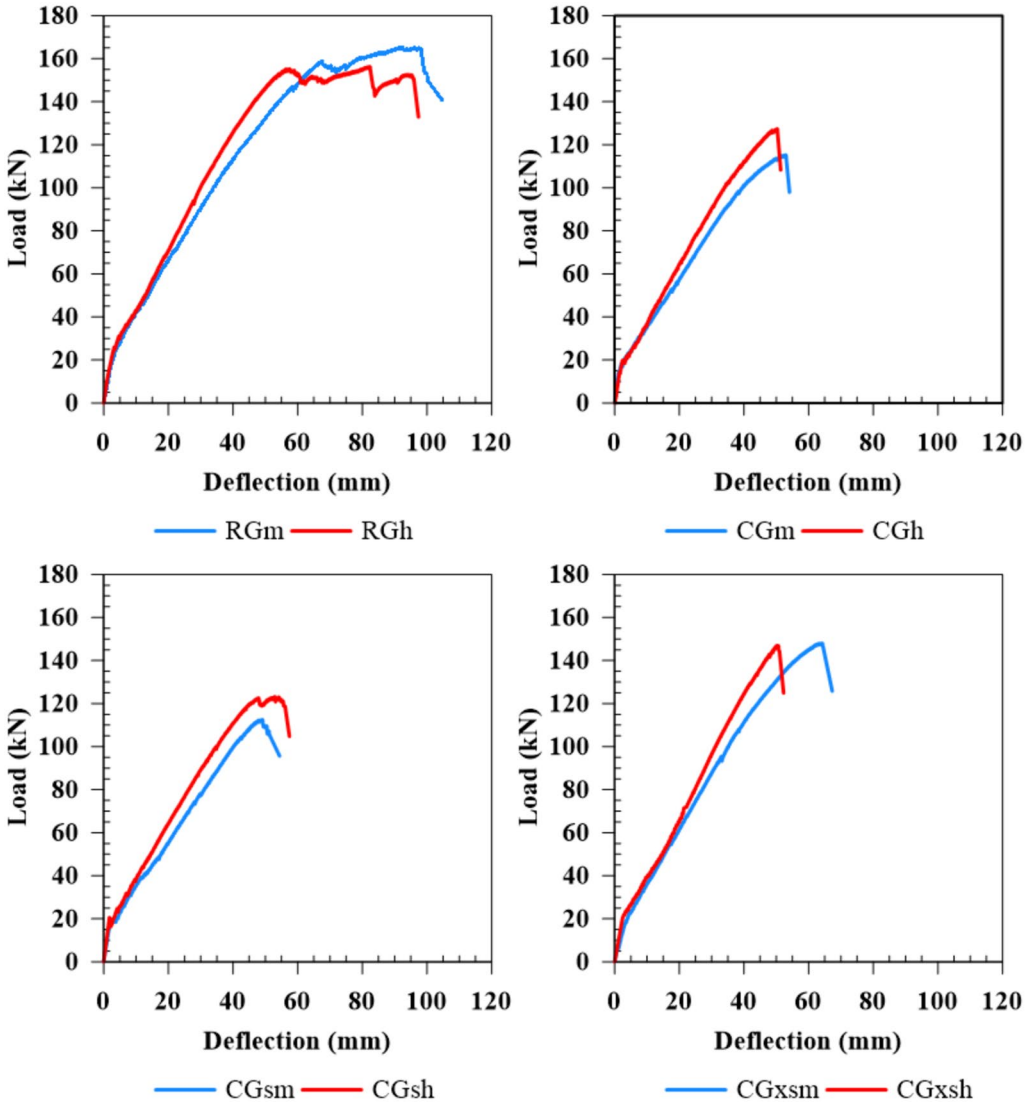

Fig. 9 Load–deflection curves of the test specimens

reinforcement (CGxsm and CGxsh), approximately 28% decrease in energy dissipation capacity, approximately 13% increase in rigididity were observed. The load capacities was not almostly changed, with a small difference of 0.70%. This situation was associated with the increase in rigidity and the limited deformability capacity of CGxsh.

Since the RGh reference specimen in the second experimental group, which has a high reinforcement ratio, did not reach its bending capacity, the calculated values of E_t/E_s and P_t/P_s were slightly overestimated compared to those in the first experimental group. Detailed evaluations of the load capacity, ductility (curvature) and strain analysis for the specimens in the second group are provided in the fourth section (Analytical Study).

4 Analytical Study

4.1 Flexural Capacities and Stress–Strain Responses

The bending capacities of tested beams were calculated using two different codes [ACI 440.1R-15, 2015 and CSA S806-12, 2012] along with Todeschini et al. (1964) concrete stress–strain model. The analytical expressions are detailed in Table 5. In Todeschini et al. (1964) concrete model, the stress $[f_c(\varepsilon_c)]$ is expressed by a single function dependent on the concrete strain (ε_c) and is given in Eq. (1). The maximum compressive stress (f'_c) corresponds to 90% of the compressive strength of standart cylinder concrete (f_c). $\beta_1(\varepsilon_c)$ and $k_2(\varepsilon_c)$ represent the width

Table 5 Flexural strength calculation principle of over-reinforced beams according to ACI 440.1R-15 (2015), CSA S806-12 (2012) codes and Todeschini (1964) concrete model

	ACI 440.1R-15 (2015)	CSA S806-12 (2012)	Todeschini model (1964)
$\boldsymbol{\rho_f}$ (reinforcement ratio)	$\rho_f = \frac{A_f}{b_w d}$ $\rho_{fb} = 0.85\beta_1 \frac{f_c}{f_{fu}} \frac{E_f \varepsilon_{cu}}{E_f \varepsilon_{cu} + f_{fu}}$	$\rho_f = \frac{A_f}{b_w d}$	$\rho_f = \frac{A_f}{b_w d}$
Coefficients of rent-angular stress block	$\beta_1 = \left\{ \begin{array}{ll} f_c \le 28MPa \rightarrow & 0.85 \\ f_c > 28MPa \rightarrow & 0.85 - \frac{0.05(f_c - 28)}{7} \ge 0.65 \end{array} \right\}$	$\alpha_1 = 0.85 - 0.0015 f_c \ge 0.67$ $\beta_1 = 0.97 - 0.0025 f_c \ge 0.67$	$\beta_1(\varepsilon_c) = \frac{\ln\left[1+\left(\frac{\varepsilon_c}{\varepsilon_o}\right)^2\right]}{\frac{\varepsilon_c}{\varepsilon_o}} k_2(\varepsilon_c) = 1 - \frac{2\left[\left(\frac{\varepsilon_c}{\varepsilon_o}\right) - a\tan\left(\frac{\varepsilon_c}{\varepsilon_o}\right)\right]}{\left(\frac{\varepsilon_c}{\varepsilon_o}\right)^2 \beta_1(\varepsilon_c)}$
$\boldsymbol{M_u}$ (Ultimate Moment Capacity)	$\rho_f > \rho_{fb} \rightarrow \left\{ \begin{array}{c} f_f = \left(\sqrt{\frac{(E_f \varepsilon_{cu})^2}{4} + \frac{0.85\beta_1 f_c}{\rho_f} E_f \varepsilon_{cu}} - 0.5 E_f \varepsilon_{cu} \right) < f_{fu} \\ M_u = \rho_f f_f \left(1 - 0.59 \frac{\rho_f f_f}{f_c}\right) b_w d^2 \end{array} \right\}$	$\alpha_1 \beta_1 f_c b_w c = A_f E_f \varepsilon_{cu} \left(\frac{d-c}{c}\right) \rightarrow c$ $f_f = E_f \varepsilon_{cu} \frac{d-c}{c} < f_{fu}$ $M_u = A_f f_f \left(d - \frac{\beta_1 c}{2}\right)$	$\beta_1(\varepsilon_{cu}) k_2(\varepsilon_{cu}) f_c b_w c = A_f E_f \varepsilon_{cu} \left(\frac{d-c}{c}\right) \rightarrow c$ $f_f = E_f \varepsilon_{cu} \frac{d-c}{c} < f_{fu}$ $M = A_f f_f \left(d - \frac{k_2(\varepsilon_{cu}) c}{2}\right)$
$\boldsymbol{\varepsilon_{cu}}$	0.003	0.0035	0.0038

A_f cross sectional area of FRP reinforcement, b_w width of beam, d effective depth of tension reinforcement, ρ_f balanced reinforcement ratio, f_c—strength of concrete, f_{fu} tensile stress of FRP reinforcement, ε_{cu} crushing strain of concrete, E_f—modulus of elasticity of FRP reinforcement, f_f stress of FRP tension reinforcement, β_1 ratio of depht of rectangular stress block to depth of neutral axis for ACI 440.1R-15 and CSA S806-12, α_1 ratio of average concrete stress to the concrete strength for CSA S806-12, $\beta_1(\varepsilon_c)$ the equivalent width of the rectangular compression block for Todeschini, $k_2(\varepsilon_c)$ equivalent depth of the rectangular compression block, ε_c compressive strain of concrete, ε_o strain value corresponding to the maximum compressive strength for Todeschini concrete model, E_c modulus of elasticity of concrete, c concrete compression depth

and depth coefficients of the equivalent rectangular stress block, respectively, and vary depending on the concrete strain (Table 5):

$$f_c(\varepsilon_c) = \frac{2f_c'\left(\frac{\varepsilon_c}{\varepsilon_o}\right)}{1+\left(\frac{\varepsilon_c}{\varepsilon_o}\right)^2} \quad (1)$$

During the calculation of load capacity and stress–strain analyses, full bond assumption between concrete and reinforcement is considered, and equality of strain values in both concrete and reinforcement at the same level is assumed. In addition, it is considered that GFRP reinforcement has a completely elastic stress–strain relationship. The calculated and the relative bending capacities, based on experimental data, are provided in Table 6. For the test specimen reaching the bending capacity (RGm), all predictions have shown a conservative approach. However, the closest results (with about a 4% difference) were obtained using the Todeschini (1964) concrete model. However, the predictions were obtained to be larger than the experimental load values for the other beams that did not reach the bending capacity.

The Todeschini (1964) concrete model were employed for stress–strain analyses of the beams. Fig. 10 shows the stress–strain diagrams, while Table 7 exhibits the concrete compressive depth (c), strains of concrete (ε_c) and GFRP reinforcement (ε_f), and curvature values (K) obtained from the analyses at ultimate load capacity. Similar to experimental studies, the analyses indicated that RGm reached the concrete crushing strain value (as reaching flexural strength), while none of the other beams achieved this. The strain values of FRP reinforcement (ε_f) for any specimen were not reached the rupture strain (ε_{fu}).

In the second experimental group, due to the RGh test element not reaching its bending capacity, a theoretical test element (RGh*t) that achieves this bending capacity has been included in Table 7 to ensure accurate evaluation. RGh reached approximately 90% of its theoretical capacity in terms of load, 85% in terms of curvature, and 85% in terms of FRP strain. RGm without openings had the highest curvature and GFRP strain values and the reinforcements utilized approximately 71% (εf/εfu) of their capacity. CGxsm with openings had larger concrete and GFRP strain values, as well as curvature, compared to RGh without openings. In addition, CGxsm had the largest values after RGh without openings in the second experimental group. Within their respective experimental groups, Among the specimens with openings, CGxsm and CGxsh had concrete strains that most closely approach the crushing strain value (εc/εcu) and had the highest curvature (Kr/Ks) values compared to the reference specimens. Similar to the experimental data, in each experimental group, the highest curvature and FRP strain values among the beams with openings were obtained in the diagonally reinforced CGxsm and CGxshh specimens. These results indicates the significance of diagonal reinforcement in GFRP-RC beams with openings.

Table 8 provides the ratios of FRP strain, curvature, and load capacity values in relation to the changes in reinforcement ratio between the two experimental groups. In over-reinforced FRP beams, the increase in reinforcement ratio does not necessarily enhance the bending capacities of beams. The main reason for this random relationship is the decrease in the strain of the FRP tension reinforcement with increasing reinforcement ratio. As shown for RGh*t/RGm* in Table 8, despite a 15% increase in the reinforcement ratio, the bending capacity increased by approximately 9%, while the FRP strain value decreased by about 8%. In addition, the curvature

Table 6 Experimental and analytical flexural strength values and ratios

Group	Beam	P_{max} (kN)	$P_{ACI\ 440}$ (kN)	$P_{CSA\ S806}$ (kN)	$P_{Tod.}$ (kN)	$P_{max}/P_{ACI\ 440}$ (%)	$P_{max}/P_{CSA\ S806}$ (%)	P_{max}/P_{Tod} (%)
1st	RGm	165.33	144.45	151.56	159.18	114.46	109.09	103.87
	CGm	115.24				79.78	76.03	72.39
	CGsm	112.52				77.90	74.24	70.69
	CGxsm	147.98				102.44	97.64	92.96
2nd	RGh	155.27	157.60	165.02	173.13	98.52	94.09	89.68
	CGh	127.37				80.82	77.19	73.57
	CGsh	123.21				78.18	74.66	71.16
	CGxsh	146.95				93.24	89.05	84.87

$P_{ACI\ 440}$ Calculated load capacity according to ACI 440.1R-15

$P_{CSA\ S806}$ Calculated load capacity according to CSA S806-12

$P_{Tod.}$ Calculated load capacity according to Todescihini concrete model

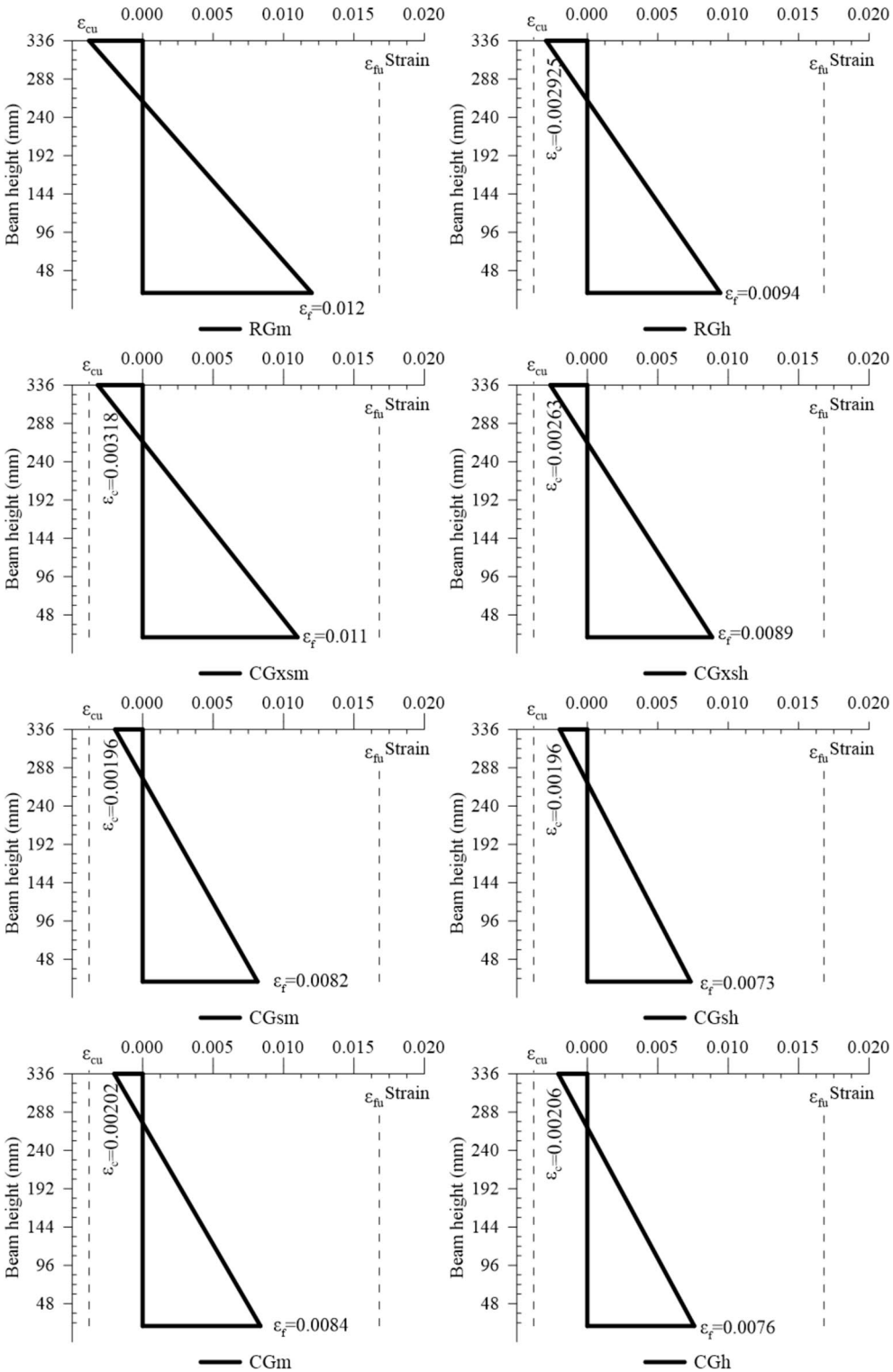

Fig. 10 Stress–strain analyses of the test specimens at ultimate load capacity

Table 7 Concrete compressive depth, strains of concrete and GFRP reinforcement, and curvature values

Group	Beam	ρ_f	C (mm)	ε_c	ε_f	$\varepsilon_c/\varepsilon_{cu}$(%)	$\varepsilon_f/\varepsilon_{fu}$(%)	K (1/m)	K_r/K_s (%)	P_{max} (kN)	P_r/P_s (%)
1st	RGm*	0.0095	75.90	0.0038	0.0120	100.00	71.43	0.050	100.00	159.18	100.00
	CGm		61.50	0.00202	0.0084	53.16	49.76	0.033	65.60	115.24	72.40
	CGsm		61.12	0.00196	0.0082	51.45	48.53	0.032	63.89	112.52	70.69
	CGxsm		70.80	0.00318	0.0110	83.68	65.48	0.045	89.71	147.98	92.96
2nd	RGh*[t]	0.0110	82.50	0.0038	0.0110	100.00	64.00	0.046	100.00	173.13	100.00
	RGh*		74.77	0.00293	0.0094	76.97	56.17	0.039	84.78	155.27	89.68
	CGh		67.46	0.00206	0.0076	54.21	45.18	0.031	67.39	127.37	73.57
	CGsh		66.65	0.00196	0.0073	51.58	43.65	0.029	63.04	123.21	71.17
	CGxsh		72.20	0.00263	0.0089	69.08	52.76	0.036	78.26	146.95	84.88

* Reference beam

RGh*[t]—therotical beam

Kr—curvature of reference beam

Ks—curvature of beam

underwent an 8% decrease. In RC beams with openings, as the reinforcement ratio increased, the load capacity reached a maximum increase of approximately 11%, while a maximum decrease of around 20% in curvature and approximately 19% in FRP strain values took place. Similarly, Abed et al. (2021) reported that as the reinforcement ratio increased for FRP-RC beams, the strain in the reinforcement decreased.

4.2 Shear Capacities

The shear capacities of tested beams without openings were calculated using two different codes (ACI 440.1R-15, (2015) and CSA S806-12, 2012). In the calculations using CSA S806-12 (2012), the inclination angle of main shear crack was assumed 45° and all material coefficients were assumed to be 1. The analytical expressions are detailed in Table 9. The calculated and the relative shear capacities, based on experimental data, are provided in Table 10. The shear strengths of reference test specimens were estimated more conservatively with CSA S806-12 (2012). RGm, which reached flexural capacity, did not reach shear capacity according to ACI 440.1R-15 (2015) ($V_{max}/V_{n\text{-}ACI\ 440}$ = 76.86%). However, it became the sole test specimen to achieve shear capacity according to CSA S806-12 (2012) ($V_{max}/V_{n\text{-}CSA\ S806}$ = 108.26%). RGh did not reach shear capacity according to both codes; however, experimental shear strengths very close to those predicted by CSA S806-12 (2012) were obtained ($V_{max}/V_{n\text{-}CSA\ S806}$ = 97.70%). The findings according to Liang et al. (2023) indicated that the shear strength predictions by CSA S806-12 (2012) for RC beams with FRP stirrups, were more precise compared to different codes. Experimental shear strengths for RC beams with openings were also more closely estimated through CSA S806-12 (2012). For the test specimens CGxsm and CGxsh, which particularly include diagonal reinforcement, the values of $V_{max}/V_{n\text{-}CSA\ S806}$ are approximately 97% and 92.5%, respectively.

Table 8 Effects of longitudinal reinforcement ratio on related parameters

(ρ_f)h/(ρ_f)m	Sh/Sm	Ratio of related parameters		
		ε_f (%)	K (%)	P_{max} (%)
1.15	RGh*[t]/RGm*	91.67	92.00	108.76
	CGh/CGm	90.47	93.94	110.52
	CGsh/CGsm	89.02	90.63	109.5
	CGxsh/CGxsm	80.90	80.00	99.3

(ρ_f)h—high reinforcement ratio

(ρ_f)m—moderate reinforcement ratio

4.3 Deflection Calculations

According to the Euler–Bernoulli theory, shear deflections in RC beams are negligible compared to bending deflections. However, in RC beams with openings, rigidity decreases, and deflections tend to increase. Although cracks and additional deflections resulting from shear effects around openings are intended to be confined by special reinforcement details, deflections due to shear reach an significant level that cannot be neglected.

4.3.1 Bending Deflection Calculation of RC Beams

The moment–area theorem has been employed for bending deflections (δ_f). δ_f for solid RC beams are calculated according to Eq. (2), while for RC beams with openings, δ_f calculated based on the model provided in Fig. 11 using Eq. (3):

Table 9 Shear strength calculation principle of RC beams according to ACI 440.1R-15 (2015) and CSA S806-12 (2012) codes

ACI 440.1R-15 (2015)		CSA S806-12 (2012)
V_c (shear strength contribution of concrete)	$V_c = 0.4\sqrt{f_c}b_w d(kd)$ $k = \sqrt{2\rho_f n_f + (\rho_f n_f)^2} - \rho_f n_f$	$V_c = 0.05\lambda\phi_c k_m k_r k_s k_a (f_c)^{1/3} b_w d_v$ $k_m = \left(\frac{V_f}{M_f} d\right)^{1/2} \leq 1$ $k_r = 1 + (\rho_f E_f)^{1/3}$ $k_s = \left(\frac{750}{450 + d}\right) \leq 1$ $k_a = \left(\frac{2.5V_f}{M_f} d\right) \leq 1$
V_{frp} (shear strength contribution of FRP stirrups)	$V_{frp} = \frac{A_{fv} f_{fv} d}{s}$ $f_{fv} = 0.004E_{fv} \leq f_{fuv}$	$V_{frp} = \frac{0.4\phi_F A_{fv} f_{fv} d_v}{s} \cot\theta$ $f_{fv} \leq 0.005E_{fv}$
V_n	$V_n = V_c + V_{frp}$	

V_n total shear strength capacity, k ratio between the depth of the neutral axis of the cracked transformed section, n_f ratio of the modulus of elasticity of FRP bars (E_f) to the modulus of elasticity of concrete (E_c), A_{fv} cross sectional area of transverse reinforcement, f_{fv} transverse reinforcement stress, E_{fv} modulus of elasticity of the FRP stirrups, s spacing of stirrups, k_m moment–shear interaction factor, k_r longitudinal reinforcement stiffness factor, k_s size effect factor, k_a effect of arc action coefficient, φ_c resistance factor for concrete, λ concrete density factor, M_f factored moment, V_f factored shear force, $d_v = max(0.9d; 0.72\,h)$ effective shear depth, Q inclination angle of main shear crack, φ_f resistance factor for FRP reinforcement

$$\delta_f = 4.374 \times 10^8 \frac{P}{E_c I} \tag{2}$$

$$\delta_f = P\left(\frac{1.698 \times 10^8}{E_c I} + \frac{2.676 \times 10^8}{E_c I_{eq}}\right) \tag{3}$$

where P and E_c represent the applied load in Newton and the modulus of elasticity of concrete in MPa, respectively. I and I_{eq} represent the moment of inertia (in mm^4) of the solid and sections with openigs, respectively. In deflection calculations, the modulus of elasticity of concrete E_c, according to the ACI (2019) calculated using the following equation:

$$E_c = 4700\sqrt{f_c} \tag{4}$$

In Eqs.(2–3) before the first cracking, the uncracked transformed moment of inertia (I_c) is utilized. In this model, the modular ratio ($n = E_f/E_c$) is used to transform all reinforcements into an equivalent concrete area. I_c is calculated for RC beams with/without openings according to Eqs. (5, 6), respectively:

$$I_c = \frac{b_w h^3}{12} + b_w h\left(\frac{h}{2} - y_1\right)^2 + (n-1) A_f\left(d - y_1\right)^2 + (n-1)A_b\left(d_b - y_1\right)^2 \tag{5}$$

Table 10 Experimental and analytical shear strength values and ratios

Group	Beam	V_{max} (kN)	$V_{n\text{-}ACI\,440}$ (kN)	$V_{n\text{-}CSA\,S806}$ (kN)	$V_{max}/V_{n\text{-}ACI\,440}$ (%)	$V_{max}/V_{n\text{-}CSA\,S806}$ (%)
1st	RGm	82.67	107.55	76.36	76.86	108.26
	CGm	57.62			53.58	75.46
	CGsm	56.26			52.31	73.68
	CGxsm	73.99			68.80	96.90
2nd	RGh	77.64	110.65	79.46	70.16	97.70
	CGh	63.69			57.56	80.15
	CGsh	61.61			55.68	77.53
	CGxsh	73.48			66.40	92.47

V_{max} Maximum experimental shear force

$V_{n\text{-}ACI\,440}$ Calculated shear strength capacity according to ACI 440.1R-15 (for RC beams without openings)

$V_{n\text{-}CSA\,S806}$ Calculated shear strength capacity according to CSA (for RC beams without openings)

$$I_c = \frac{b_w h^3}{12} + b_w h\left(\frac{h}{2} - y_1\right)^2 + (n-1)A_f\left(d - y_1\right)^2 + (n-1)A_b\left(d_b - y_1\right)^2 - \frac{b_o h_{eq}^3}{12} \quad (6)$$

where h_{eq} (equivalent opening depth) is calculated as the ratio of the circular opening area to the opening width (b_o). In other words, the circular opening area has been transformed into an equivalent rectangular area at the center of the section. d and d_b represent the depths from the outermost compression face to the center of the tensile and compressive reinforcements, respectively. y_1 shows the depth of the transformed section center relative to the outermost compression face. A_f and A_b symbolizes the total tensile and compressive reinforcement areas, respectively.

The effective moment of inertia expression by Bischoff (2005) (Eq. 7) has been employed for the calculation of bending deflections after the first cracking:

$$\frac{1}{I_{ef}} = \left(\frac{M_{cr}}{M_a}\right)^2 \frac{1}{I_c} + \left[1 - \left(\frac{M_{cr}}{M_a}\right)^2\right] \frac{1}{I_{cr}} \quad (7)$$

where M_{cr} and M_a represent the first cracking and the applied moments, respectively. The experimental first-cracking loads have been used in the calculation of deflections for each beam. I_{cr} exhibits the cracked moment of inertia and is calculated for both RC beams with and without openings using the following equation:

$$I_{cr} = \frac{b_w c^3}{3} + nA_f(d-c)^2 + (n-1)A_b(c-d_b)^2 \quad (8)$$

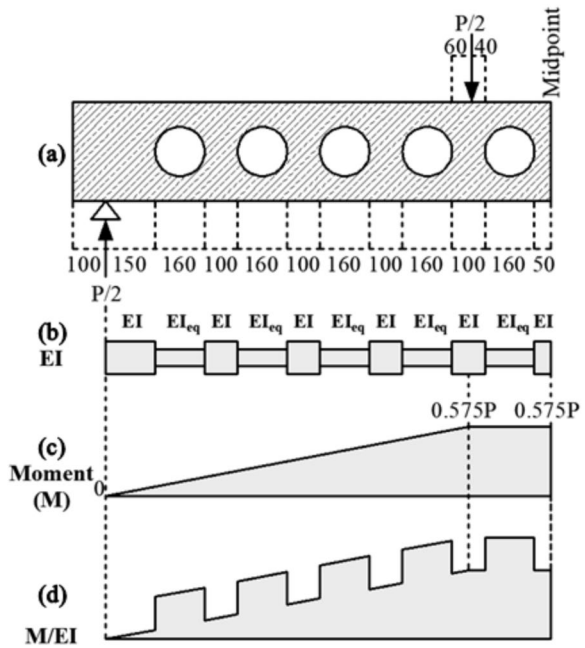

Fig. 11 **a** Details, **b** flexural rigidity model, **c** bending moment diagram, **d** M/EI diagram for the beams

4.3.2 Shear Deflection Calculation of RC Beams with Openings

Mansur and Tan (1999) developed Eq. (9) to calculate deflections (δ_v) resulting from shear forces around openings in RC beams with limited number of web openings:

$$\delta_v = \frac{V l_e^3}{12 E_c (I_u + I_l)} \quad (9)$$

where V represents the shear force, while l_e symbolizes the effective distance between the plastic hinges. I_u and I_l are the effective moments of inertia of the upper and lower chords, respectively. It was assumed for deflection calculations, the upper chord remains uncracked, while the lower chord is considered cracked. The uncracked and cracked moments of inertia expressions were employed for the calculation of I_u and I_l, respectively.

l_e is the effective length of the hinging location which is utilized instead of the actual length (l_o). The main reason for this is to include the deflections arising from additional rotations in the beam due to cracks at the end of the chords. Mansur and Tan (1999) suggested Eq. (10) for l_e using the experimental data of Huang (1989) and Mansur et al. (1992):

$$l_e = \frac{l_o}{1 - \left(\frac{h_{eq}}{h}\right)^{1.5}} \quad (10)$$

Aykaç and Yılmaz (2011), Aykaç et al., (2013, 2014) indicated, similar to the present study, that the plastic hinge mechanism does not occur in RC beams with circular openings. Kalkan et al. (2021) on the other hand, studied on deflection calculations in RC beams with openings. l_o was proposed by calculating the value by considering the length of the group of openings remaining under the maximum shear load in RC beams that Virendeel panel action type of shear failure does not occur, According to this approach, in the present study, a value of 940 mm for l_o has been included in the calculations to encompass four openings and the posts between them. In addition, in the group of openings located in the shear zone, the shear force is constant and equal to $P/2$. Accordingly, shear deflections have been calculated taking into account $V = P/2$ as in Eq.(9).

4.3.3 Total Deflection Calculation of RC Beams with Openings

Kalkan et al. (2021) demonstrated that the total deflection resulting from shear and bending ($\delta = \delta_f + \delta_v$) deviates from experimental data in RC beams with regular web openings. In this context, Kalkan et al. (2021) utilized experimental studies available in the literature to develop the principle of deflection equality at the service load level and proposed magnifying the total deflections (δ) for each geometry of opening with a different coefficient. The coefficient (α) proposed for RC beams with circular openings is 1.18. The increased total deflection (δ^*) values have been calculated [Eq. (11)] with the coefficient of α *(1.18)* Experimental and analytical load–deflection curves of the beams are presented in Fig. 12. In Fig. 12, "(e)" represents the experimental curve. "(f)", "(f + s)" and "*" are the predicted curves correspond to only bending (δ_f), the total of bending and shear (δ), the increased total deflection (δ^*) values, respectively.

Kalkan et al. (2021) calculated the coefficient α considering long-term loads ($0.60f_{ck}$) for serviceability limit state as specified in Eurocode 2 (CEN, 2004). f_{ck} represents the characteristic compressive strength of concrete. Accordingly the strain of concrete, deflection and load values for the serviceability limit state were estimated using the Todeschini (1964) concrete model in the present study. The experimental and anayltical deflections at the service load level are given in Table 11.

Deflections at the service load level were predicted with an average approximate accuracy of about 97% (Table 8).

$$\delta^* = \alpha \times \delta = \alpha \times \left(P \left(\frac{1.698 \times 10^8}{E_c I} + \frac{2.676 \times 10^8}{E_c I_{eq}} \right) + \frac{P/2(l_e/2)^3}{12E_c(I_u + I_l)} \right) \tag{11}$$

5 Conclusions

The present study is an attempt to unfold the flexural behavior of RC beams with multiple regular web openings and non-corroding GFRP reinforcement. The study focused on the load–deflection behavior of these beams with a special emphasis on the flexural reinforcement ratio and special reinforcement schemes (short stirrups in the chords and diagonal reinforcement around the openings) against various shear failure modes (beam-type, frame-type and Vierendeel panel action) in RC beams with openings. Within this scope, a total of 8 RC beams, including two reference ones, were tested to failure under four-point bending. The effects of these parameters on the failure mode, load and energy dissipation capacities were examined. In addition, the prediction of load–deflection curves of the beams and stress–strain analyses have also been conducted. Finally, the experimental failure loads of the beams were compared to the analytical estimates according to various structural concrete codes. The obtained results are listed as follows:

- In each test group, the rigidity, load-carrying capacity, and energy dissipation capacities of the references are the highest within their respective test groups. However, in specimens with openings, decreases are observed in all mentioned parameters.
- The only specimen reaching the flexural capacity is RGm. In GFRP-RC beams with regular web openings, concrete crushing in the diagonal direction and bond failure at the level of openings were observed simultaneously in the lower and upper chords in the shear zone. Therefore, none of them could reach the flexural capacity. It can be attributed to the low depth of the chords, the contribution of low shear strength of the short individual stirrups, and the low dowel action of the longitudinal GFRP reinforcement. With the beginnging of concrete crushing in reference specimens, the load–deflection curve flattens horizontally, whereas in specimens with openings, the load values dropped abruptly due to brittle shear failure.
- With an increase in the reinforcement ratio, the rigidity of RC beams with openings has shown a slight increase. Generally, there is a tendency for an increase in both the load-carrying capacity and energy dissipation capacities. However, exceptions to this general trend include RGh not to reach the flexural capacity and the lower energy consumption of CGxsh compared to CGxsm in cross-reinforced specimens.
- As a result of stress–strain analyses, it has been demonstrated that the maximum strain values in both concrete and FRP reinforcement, as well as the maximum curvature values, occur in the reference test specimens. However, these analyses have also showed that the use of diagonal reinforcement in RC beams with openings provides significant strength and strain capacity as compared the other RC beams with openings.
- It has been concluded that the presence of short stirrups in the posts has no effect on the rigidity, load-carrying capacity, and energy dissipation capacities. This situation can be explained by the low confinement effect of the short stirrups.

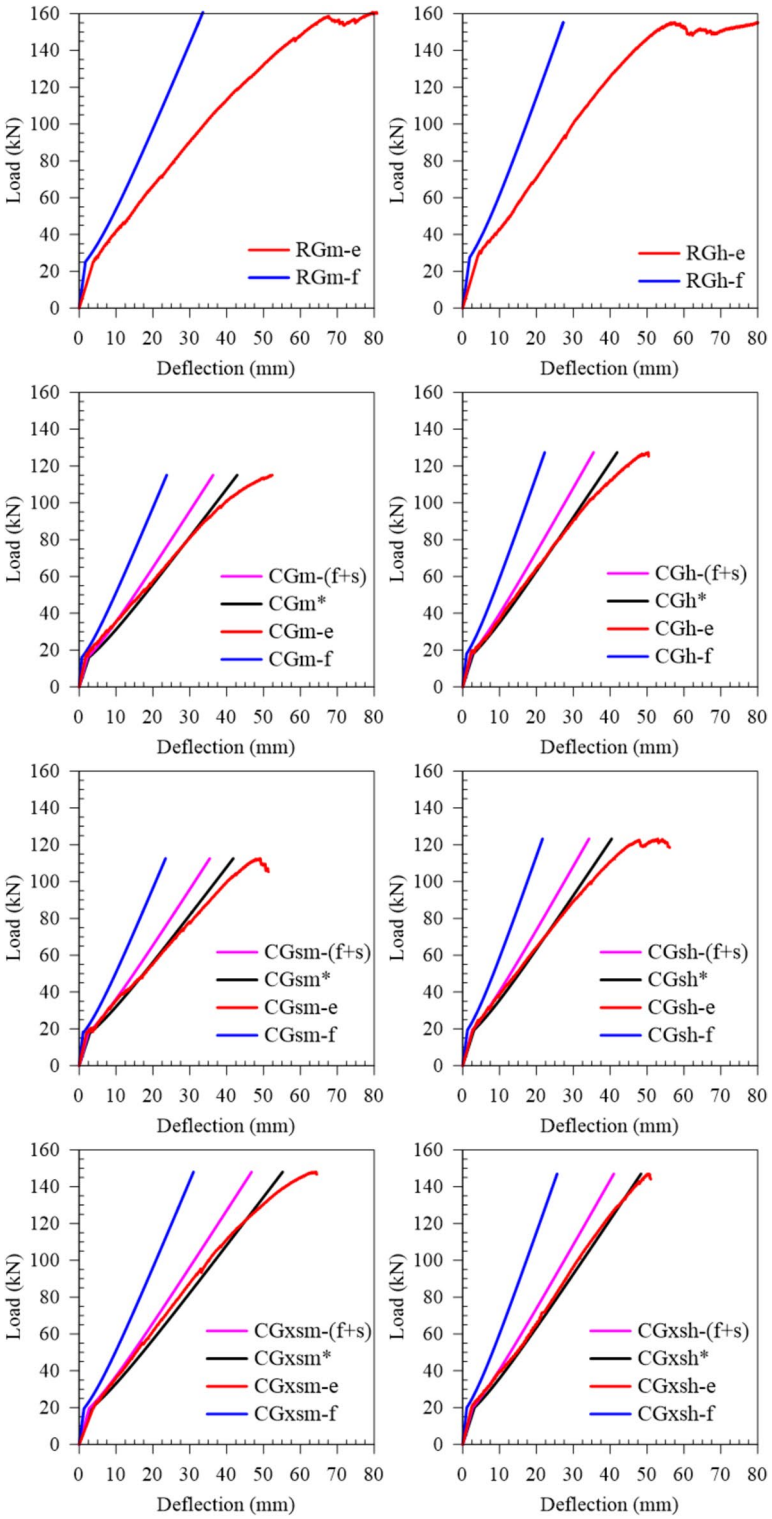

Fig. 12 Experimental and predicted load–deflection curves

Table 11 Experimental and anayltical deflections at the service load level

Group	Beam	P_s (kN)	$\delta_{s\text{-}exp}$ (mm)	$\delta_{s\text{-}an}$ (mm)	$\delta_{s\text{-}exp}/\delta_{s\text{-}an}$ (%)
1st	CGm	53.03	18.08	18.73	96.53
	CGsm	53.03	18.99	18.73	101.39
	CGxsm	53.03	17.51	18.73	93.49
2nd	CGh	58.15	17.77	18.28	97.21
	CGsh	58.15	17.62	18.28	96.39
	CGxsh	58.15	17.65	18.28	96.55

P_s load at service limit state

$\delta_{s\text{-}exp}$ experimental deflection at service limit state

$\delta_{s\text{-}an}$ analytical deflection at service limit state

The present study constitutes the first stage of the research on RC beams with openings against corrosion effects. In the second stage, the use of new non-corrosive materials with higher shear strength as shear reinforcement is planned. In addition, accelerated corrosion tests will be included in the subsequent stages of research to determine the effects of corrosion on structural behavior.

6 Future Research Needs

FRP reinforcement is generally more costly than traditional steel reinforcement. Due to their great corrosion and chemical resistance, FRP reinforcing bars can significantly reduce maintenance costs over time. Therefore, FRP bars are widely used in aggressive environments such as the conditions in the marine structures, bridges, and chemical plants. FRP bars are lighter than steel bars, making transportation and installation of these bars easier. However, they are also more brittle and must be handled with care. Unlike steel, GFRP bars cannot be easily bent or cut on-site. Special tools and pre-shaped bars (stirrups) are required. Due to the different mechanical properties of GFRP bars, some adjustments in structural design may be needed. Many countries do not have specific structural codes and standards for the use of FRP reinforcement. Therefore, project managers and engineers must ensure compliance with local codes.

FRP reinforcement research topic involves gaps such as long-term durability, economic analysis and large-scale corrosion tests. In addition, structural health monitoring for diagnosing damage in RC structural elements have become popular recently. This topic is also important for structural members reinforced with FRP and it has the potential to be investigated in the future studies, as the one conducted by Chalioris et al. (2021). In this study, a low-cost wireless monitoring system was used to detect concrete cracking and steel reinforcement yielding and the effectiveness of this method was shown. In order for the use of FRP reinforcement to become more widespread and increase its prevalence, similar innovative studies regarding FRP-reinforced structural elements are necessary.

The current codes predominantly address GFRP (extensive research has been conducted on GFRP-related topics) and a large percentage of all published papers is related to the performance of FRP in concrete beams and columns. Therefore, further research is necessary to establish a basis for incorporating the other types of FRP and other structural elements into future code revisions.

Acknowledgements
The study was carried out within the scope of the project with the number of 2022/065 supported by Kırıkkale University Scientific Research Projects Unit. The financial support provided by this unit is gratefully acknowledged.

Author contributions
Saruhan Kartal: Conceptualization, Data collection and analysis, Writing—original draft, Writing—review & editing, Validation, Methodology. Emin Kısıklı: Data collection and analysis, experimental study.

Funding
This investigation was supported by the Kırıkkale University Scientific Research Projects Unit (Grant No: 2022/065).

Availability of data and materials
All data generated or analyzed during this study are included in this published article and the data file could be offered by contacting the corresponding author if needed.

Declarations

Ethics approval and consent to participate
Not applicable.

Consent for publication
The manuscript is approved by all authors for publication. The author declares that the work described was original research that has not been published previously, and not under consideration for publication elsewhere, in whole or in part.

Competing interests
The authors declare no competing interests.

Received: 18 March 2024 Accepted: 5 August 2024
Published online: 08 November 2024

References

Abdel-Kareem, A. H. (2014). Shear strengthening of reinforced concrete beams with rectangular web openings by FRP Composites. *Advances in Concrete Construction, 2*(4), 281. https://doi.org/10.12989/acc.2014.2.4.281

Abed, F., Al-Mimar, M., & Ahmed, S. (2021). Performance of BFRP RC beams using high strength concrete. *Composites Part c: Open Access, 4*, 100107. https://doi.org/10.1016/j.jcomc.2021.100107

ACI (American Concrete Institute) (2019) ACI 318-19M: Building code requirements for structural concrete and commentary. ACI, Farmington Hills, MI, USA.

ACI-440, Guide for the Design and Construction of Structural Concrete Reinforced with Fiber-Reinforced Polymer (FRP), 2015: ACI 440. 1R-15, American Concrete Institute, Farmingtons, Hills, MI.

Almusallam, T., Al-Salloum, Y., Elsanadedy, H., Alshenawy, A., & Iqbal, R. (2018). Behavior of FRP-strengthened RC beams with large rectangular web openings in flexure zones: Experimental and numerical study.

International Journal of Concrete Structures and Materials, 12(1), 1–28. https://doi.org/10.1186/s40069-018-0272-5

Amin, S., Elwan, S. K., Elzeiny, S., Hamad, M., & Deifalla, A. (2021). Numerical modeling the effect of an opening on the behavior of exterior beam-column connections under cyclic loading. *Journal of Building Engineering, 40*, 102742. https://doi.org/10.1016/j.jobe.2021.102742

Aykac, B., Aykac, S., Kalkan, I., Dundar, B., & Can, H. (2014). Flexural behavior and strength of reinforced concrete beams with multiple transverse openings. *ACI Structural Journal, 111*(2), 267–277.

Aykac, B., Kalkan, I., Aykac, S., & Egriboz, Y. E. (2013). Flexural behavior of RC beams with regular square or circular web openings. *Engineering Structures, 56*, 2165–2174. https://doi.org/10.1016/j.engstruct.2013.08.043

Aykac, S., & Yilmaz, M. (2011). Behaviour and strength of RC beams with regular triangular or circular web openings. *Journal of the Faculty of Engineering and Architecture of Gazi University, 26*(3), 711–718.

Bischoff, P. H. (2005). Reevaluation of deflection prediction for concrete beams reinforced with steel and fiber reinforced polymer bars. *Journal of Structural Engineering, 131*(5), 752–767. https://doi.org/10.1061/(ASCE)0733-9445(2005)131:5(752)

Cairns, J., Plizzari, G. A., Du, Y., Law, D. W., & Franzoni, C. (2005). Mechanical properties of corrosion-damaged reinforcement. *ACI Materials Journal, 102*(4), 256.

Chalioris, C. E., Kytinou, V. K., Voutetaki, M. E., & Karayannis, C. G. (2021). Flexural damage diagnosis in reinforced concrete beams using a wireless admittance monitoring system—tests and finite element analysis. *Sensors, 21*(3), 679. https://doi.org/10.3390/s21030679

Coccia, S., Imperatore, S., & Rinaldi, Z. (2016). Influence of corrosion on the bond strength of steel rebars in concrete. *Materials and Structures, 49*, 537–551. https://doi.org/10.1617/s11527-014-0518-x

Coronelli, D. (2002). Corrosion cracking and bond strength modeling for corroded bars in reinforced concrete. *Structural Journal, 99*(3), 267–276. https://doi.org/10.14359/11910

CSA, Code for the Design and Construction of Building Structures with Fibre-Reinforced Polymers, in CAN/CSA/S806–12, Canadian Standard Association, Toronto, Ontario, Canada, 2012, p. 198.

Di Carlo, F., Meda, A., & Rinaldi, Z. (2023). Structural performance of corroded RC beams. *Engineering Structures, 274*, 115117. https://doi.org/10.1016/j.engstruct.2022.115117

Elansary, A. A., Aty, A. A. A., Abdalla, H. A., & Zawam, M. (2022, March). Shear behavior of reinforced concrete beams with web opening near supports. In Structures (Vol. 37, pp. 1033–1041). Elsevier. https://doi.org/10.1016/j.istruc.2022.01.040

El-Kareim, A., Arafa, A., Hassanin, A., Atef, M., & Saber, A. (2020, October). Behavior and strength of reinforced concrete flanged deep beams with web openings. In Structures (Vol. 27, pp. 506–524). Elsevier. https://doi.org/10.1016/j.istruc.2020.06.003

Elsanadedy, H. M., Al-Salloum, Y. A., Almusallam, T. H., Alshenawy, A. O., & Abbas, H. (2019). Experimental and numerical study on FRP-upgraded RC beams with large rectangular web openings in shear zones. *Construction and Building Materials, 194*, 322–343. https://doi.org/10.1016/j.conbuildmat.2018.10.238

European Committee for Standardization. EN 1992-1-1: Design of Concrete Structures (Eurocode 2)—Part 1–1: General Rules and Rules for Buildings; European Committee for Standardization (CEN): Brussels, Belgium, 2004.

Huang, L. M. (1989). Concrete beams with small openings under bending and shear. MEng Thesis, National Univer. of Singapore.

Imperatore, S., & Rinaldi, Z. (2009). Mechanical behavior of corroded rebars and influence on the structural response of R/C elements. Concrete Repair, Rehabilitation and Retrofitting II, Alexander et al.(eds.), Taylor & Francis Group, London, 489–495.

Imperatore, S., Rinaldi, Z., & Drago, C. (2017). Degradation relationships for the mechanical properties of corroded steel rebars. *Construction and Building Materials, 148*, 219–230. https://doi.org/10.1016/j.conbuildmat.2017.04.209

Kalkan, I. (2014). In-plane flexural behavior of reinforced concrete beams with regular openings. *Journal of the Faculty of Engineering and Architecture of Gazi University, 29*(1), 155–163.

Kalkan, I., Ceylan, E., Kartal, S., & Baran, M. (2021). Deflections of reinforced concrete beams with transverse openings of different geometries. *Structural Engineering and Mechanics, 80*(3), 323. https://doi.org/10.12989/sem.2021.80.3.323

Kartal, S. (2024, March). Flexural behavior of RC beams with multiple parallelogram openings. In Structures (Vol. 61, p. 106041). Elsevier. https://doi.org/10.1016/j.istruc.2024.106041

Kartal, S., Kalkan, I., Beycioglu, A., & Dobiszewska, M. (2021). Load-deflection behavior of over-and under-reinforced concrete beams with hybrid FRP-steel reinforcements. *Materials, 14*(18), 5341. https://doi.org/10.3390/ma14185341

Kartal, S., Kalkan, I., Mertol, H. C., & Baran, E. (2023). Influence of the proportion of FRP to steel reinforcement on the strength and ductility of hybrid reinforced concrete beams. *European Journal of Environmental and Civil Engineering, 27*(12), 3546–3565. https://doi.org/10.1080/19648189.2022.2143429

Koura, M. M., Tahwia, A. M., & Matthana, M. H. (2024). Influence of macro-synthetic fibers on the flexural behavior of high strength concrete beams reinforced with GFRP bars. *Mansoura Engineering Journal., 49*(4), 4. https://doi.org/10.58491/2735-4202.3205

Kytinou, V. K., Kosmidou, P. M. K., & Chalioris, C. E. (2022). Numerical analysis exterior RC beam-column joints with CFRP bars as beam's tensional reinforcement under cyclic reversal deformations. *Applied Sciences, 12*(15), 7419. https://doi.org/10.3390/app12157419

Liang, X., Peng, J., & Ren, R. (2023). A state-of-the-art review: Shear performance of the concrete beams reinforced with FRP bars. *Construction and Building Materials, 364*, 129996. https://doi.org/10.1016/j.conbuildmat.2022.129996

Lu, W. Y., Yu, H. W., Chen, C. L., Liu, S. L., & Chen, T. C. (2015). High-strength concrete deep beams with web openings strengthened by carbon fiber reinforced plastics. *Computers and Concrete, 15*(1), 21–35. https://doi.org/10.12989/cac.2015.15.1.021

Mansur, M. A. (1998). Effect of openings on the behaviour and strength of R/C beams in shear. *Cement and Concrete Composites, 20*(6), 477–486. https://doi.org/10.1016/S0958-9465(98)00030-4

Mansur, M. A. (1999). Design of reinforced concrete beams with small openings under combined loading. *ACI Structural Journal, 96*(5), 675–681.

Mansur, M. A. (2006). Design of reinforced concrete beams with web openings. In Proceedings of the 6th Asia-Pacific structural engineering and construction conference (ASPEC 2006) (pp. 5–6). Malaysia: Kuala Lumpur.

Mansur, M. A., & Tan, K. H. (1999). *Concrete beams with openings: analysis and design* (Vol. 20). CRC Press.

Mansur, M. A., Huang, L. M., Tan, K. H., & Lee, S. L. (1992). Deflections of reinforced concrete beams with web openings. *Structural Journal, 89*(4), 391–397. https://doi.org/10.14359/3019

Mansur, M. A., Lee, Y. F., Tan, K. H., & Lee, S. L. (1991). Tests on RC continuous beams with openings. *Journal of Structural Engineering, 117*(6), 1593–1606. https://doi.org/10.1061/(ASCE)0733-9445(1991)117:6(1593)

Nie, X. F., Zhang, S. S., Chen, G. M., & Yu, T. (2020). Strengthening of RC beams with rectangular web openings using externally bonded FRP: Numerical simulation. *Composite Structures, 248*, 112552. https://doi.org/10.1016/j.compstruct.2020.112552

Nie, X. F., Zhang, S. S., Teng, J. G., & Chen, G. M. (2018). Experimental study on RC T-section beams with an FRP-strengthened web opening. *Composite Structures, 185*, 273–285. https://doi.org/10.1016/j.compstruct.2017.11.018

Salih, R., Zhou, F., Abbas, N., & Khan Mastoi, A. (2020). Experimental investigation of reinforced concrete beam with openings strengthened using FRP sheets under cyclic load. *Materials, 13*(14), 3127. https://doi.org/10.3390/ma13143127

Tan, K. H., & Mansur, M. A. (1996). Design procedure for reinforced concrete beams with large web openings. *Structural Journal, 93*(4), 404–411. https://doi.org/10.14359/9699

Tan, K. H., Mansur, M. A., & Wei, W. (2001). Design of reinforced concrete beams with circular openings. *Structural Journal, 98*(3), 407–415. https://doi.org/10.14359/10229

Todeschini, C. E., Bianchini, A. C., & Kesler, C. E. (1964). Behavior of concrete columns reinforced with high strength steels. *Journal Proceedings, 61*(6), 701–716. https://doi.org/10.14359/7803

Wei, B., He, X., Zhou, M., Wang, H., & He, J. (2024). Experimental study on flexural behaviors of FRP and steel bars hybrid reinforced concrete beams. *Case Studies in Construction Materials, 20*, e02759. https://doi.org/10.1016/j.cscm.2023.e02759

Wojdak, R. (2013). Structural analysis of a failured RC beam with openings in a building under construction. *Czasopismo Techniczne. Budownictwo, 110*(2-B), 157–168.
Yang, K., Wu, Z., Zheng, K., & Shi, J. (2024). Design and flexural behavior of steel fiber-reinforced concrete beams with regular oriented fibers and GFRP bars. *Engineering Structures, 309*, 118073. https://doi.org/10.1016/j.engstruct.2024.118073

Publisher's Note

Saruhan Kartal is an assistant professor at Kirikkale University, Department of Civil Engineering.

Emin Kısıklı has a master's degree from Kirikkale University, Instute of Science.